Applied radiation physics techniques for diagnostic evaluation of the plasma wind and thermal protection system critical parameters in aerospace re-entry

New Infrared and Gamma radiation techniques for Thermal Protection Systems Temperature and Wear Rate

Abstract

The conditions reached by a vehicle during Earth's atmosphere or from interplanetary trajectories re-entry are the most critical space mission phases for materials used as Thermal Protection Systems (TPSs), since space capsule and spacecraft surfaces have to withstand extremely high heat fluxes and loads due to the high energy shock waves during the deceleration phase, which can produce surface temperature of the order of 2000 °C. Passive and active TPSs are employed to protect the inner cold structure of hypersonic space vehicles made of aluminium or metallic alloys. Passive TPS are classified as reusable or single use (ablative). As a matter of fact one of the most complex issues during a hypersonic Plasma Wind Tunnel test campaign is to measure and monitor the high heat fluxes, the correlated surface temperatures and the wear rate (i.e., linear recession rate) affecting the behavior of TPS materials representative of space vehicle subcomponents.

The purpose of the paper is, after having widely reviewed the methodologies used in the aerospace field today, to present the CIRA novel contactless diagnostics for simultaneously temperature and wear rate determinations based respectively on Dual Color infrared thermography and on radioactive Surface ion beam Layer Implantation (SLI) techniques. Furthermore possible future validation tests are outline, through the use of the intense ^{7}Be radioactive beam available at the 3MV Pelletron tandem accelerator of the CIRCE Laboratory and the GHIBLI plasma wind tunnel facility at CIRA.

1. Introduction

The high thermal loads to which the Thermal Protection System (TPS) materials are subject during the re-entry phase in atmosphere from Earth's orbit or from interplanetary trajectories are due to the hot plasma gases downstream the shock waves generated from the extreme deceleration in front of TPSs vehicles. The gases are highly excited and heated to values up to 10000 K immediately downstream the shock waves; the TPS surfaces are then heated by the gases through convection and radiation, producing very high wall heat fluxes and so high temperatures (TPS surface temperatures reach values of about 2000 °C). The excited species (molecules, atoms, ions and electrons) created in this phase diffuse in the boundary layer and react with the TPS materials with the final effect to degrade them.

- *TPS Materials*

The TPSs are the class of materials and substructures employed to protect the assembles of space vehicles and to guarantee their integrity. They are commonly divided in two main categories, mainly reusable and ablative ones.

Ultra High Temperature Ceramics (UHTCs) and Ceramic Matrix Composites (CMCs) are widely employed as reusable TPSs [1-6] and their use is preferred when no material consumption is required as well as no changes of the aerodynamic shapes and profiles. Based on carbon fiber carbon matrix composites (C/C) and ceramic tiles, the heatshield of the Space Shuttle is the most popular example of reusable TPS [7]. Ceramic composites based on transition metal diborides such as ZrB_2 and HfB_2 and silicon carbide (SiC) are commonly referred as UHTCs. During the re-entry step in Earth's atmosphere, this class of materials is subject to oxidation processes associated to the formation of oxide scale. The physical stability of these new surface species depends on total external pressure, partial oxygen pressure, and temperature [1, 8-10]. Also CMCs are subjected to oxidation processes according to active regime or passive one mainly depending on partial oxygen pressure and temperature [11-13].

Composites with a matrix based on cured organic resin systems reinforced by fibres such as carbon or silica fibres are common ablative materials for TPSs since 1960's, when they were used in the Apollo program [14-16]. For example, Carbon-Phenolic Composites (CPCs, phenolic matrix composites reinforced with carbon fibres) have been extensively used as ablative materials, see e.g. [17-27]. During extraterrestrial re-entry phases, different modifications are possible depending on the atmosphere chemical composition. The ablation phenomenon of a charring heat shield material has been studied since the 1960's [28, 29]. When ablative materials reach very high temperatures at very high heating rates, they undergo complex endothermic processes of chemical decomposition concurrently with the production of pyrolytic gases, melting, sublimation, charring and evaporation, which contribute to stabilize the surface temperature by thermal dissipation. When molecular and atomic oxygen are present (e.g. during Earth's atmosphere re-entry phase), oxidation processes are also observed during ablation phenomena. If the carbonaceous char layer formed during the ablation shows a compact and uniform structure, it can protect the inner layers of the material respect to oxidation processes. The mechanical erosion of the superficial char due to the free stream becomes, therefore, a further critical issue: only a relative compact and mechanically stable char layer can act as protective blanket by reducing the diffusion rate of reacting species (e.g. atomic species such as oxygen).

Therefore both classes of TPS materials are subject to chemical and morphological transformations during a re-entry phase. In this scenario advanced, non-intrusive and online techniques have been (and still are) under developed to characterize the behaviour of the TPS materials subjected to these tremendous thermal and mechanical stresses.

- *Surface temperature diagnostic methodologies*

To characterize the behavior of TPS materials, these are tested in facility able to experimentally simulate the re-entry phase, such as Plasma Wind Tunnel (PWT). Monitoring

surface temperature during this kind of tests requires techniques and tools able to follow strong spatial and temporal thermal gradients. In this regard, several techniques have been developed to measure point-like objects temperature, in severe conditions, with different degrees of accuracy such as thermocouples or by means of inferential way using IR pyrometers [30], but the IR thermography is preferred due to its great potential as contactless, real time and full filed inspection method to map temperature surfaces [31].

The processes to which the TPS materials are subjected makes difficult to define a right emissivity value since, due to the change of the material chemical features during the ablation and erosion processes, it changes during the heating phase. This parameter is crucial for the determination of the two dimensional temperature maps though IR (Infra-Red) thermography since a wrong setting gives wrong information about the temperature measurement, that lead to completely incorrect temperature values. This process (i.e. the emissivity right setting) becomes more difficult as more innovative and, hence, less characterized the material is.

To overcome problems concerning emissivity, researcher suggested several solutions. For example Maldague [X. P.V. Maldague, Theory and practice of infrared technology for nondestructive testing, Wiley Interscience 2001.] proposes, among the others, black painting, thermal transfer imaging and multi-wavelength pyrometry. Black painting and thermal transfer imaging are not practicable solutions in PWT due to the sever conditions which characterize tests.

The application of the multispectral method by using thermography is a relative recent matter. In this case, the main issue concerns with the realization of a system capable to acquire the spectral radiation at different wavelengths for each pixel of the observed area. Zhang et al. [32] used a conceptual design for a multi-channel system for multispectral thermography and demonstrated an uncertainty less than 10% over a large range of temperatures. Mölleman [33] showed the potential of dual colour thermography, using narrow pass band filters. It found

that the technique is more sensible in the middle wave (MW) region and underlined the importance of filters optimization and Savino et al. [34] developed and validated up to 650°C an analytical model to determine the feasibility of the surface temperatures technique with uncertainty less then 10 % in MW range.

The dual color IR technique presented in this work takes also as advantage the use of filters working at wavelength (around 2μm) near to NIR (Near Infra Red range), which is the spectral window where dual color pyrometers usually work, using just one thermocamera and implemented in the mechanically balanced wheel rotating at high frequency (up to 100 Hz) synchronized with detector of the camera. This kind of set up allows temperature measurements maps at unsteady conditions with uncertainty between 5 and 10 %.

- *Wear rate methodologies*

At the same time the TPS wear rate (i.e., linear recession rate) provides accurate knowledge on the material shape change due to the interaction with the heat fluxes and is one of the main parameters for the evaluation of the performance of ablative TPS.. The evaluation of the thickness wear and the related recession rate are commonly evaluated comparing the samples thickness before and after the test and then calculating the recession rate assuming a stationary process. This is a rough approximation which leads to an average value for the parameter and not gives any information about the temporal evolution of the recession process. In the last years researchers worked to find an in-situ method which allows to detect the recession rate during the tests. Among the proposed methods there are side-on camera measurements, 3D photo-reconstruction method and laser-based recession technique which are not intrusive optical method and do not require modifications of the tested articles. Other explored solutions are recession sensors and spectroscopic methods.

Regarding the side on camera method, Helber et al. [35, 36] used a High Speed Camera (HSC) for tests in VKI Plasmatron facility and the 1-D recession rate can be easily detected

(with a sensitivity of about 20 μm) by a HSC since the penetrated surface leaves a brittle char layer. The pixel/mm conversion was determined using a mm-resolved chess-board and the volume loss was estimated assuming axisymmetric recession and integrating the exact profile. The sensibility of the technique used by Helber et al. depends on the HSC resolution and has the pixel dimension (about 20 μm)

Schairer et al. [37] demonstrated the applicability of the 3-D photo reconstruction method, based on stereo photogrammetry; using high resolution video images of the ablating surface from at least two directions, software automatically reads the sequences of images and, by successive image cross correlation, tracks the deformation of a surface grid that conforms to the shape of the test article. with a sensitivity of dozens of μm [38]. However this kind of techniques can hardly be used for hypersonic jets in on-ground facilities, since in that case the models are surrounded by shock wave whose emitted radiation tends to saturate the detector of the fast cameras usually sensitive in the visible spectral range.

The laser based recession technique differently from the upper two optical methods requires an external light source. Sherrouse et al. [39] developed and demonstrated the applicability of a recession rate monitoring technique able to measure 1D-recession by mean of lines of laser light projected at a given angle onto the surface of the material under test. One dimensional profiles have been obtained at a rate of 30 Hz with a sensitivity of about 0.13 mm [40]. The implementation of this technique in the hypersonic plasma wind tunnel can be not foregone since the windows of the optical access must be transparent at the working laser wavelength and a not optimized window in the spectral range can affect the energy of the beam directed inside the test chamber and the obtained technique results. Spectroscopy is one of the newest technique applied for remote recession measurements; Butler et al. [41] developed and tested this method with Phenolic Impregnated Carbon Ablator (PICA) seeded with a tracer material with a distinguishable spectral signature, at a known depth and position. When the material recession reaches the seeding depth the seed material is gasified and the spectral signal is

detected by optical emission spectroscopy. A rate of materiel recession or charring can be determined based upon the properties of the seed material and the time resolved spectra. The sensibility of the spectroscopic method is variable and depends on tracer material properties and moreover can drastically change the mechanical properties of the material investigated.

A part from optical methods the recession rate can be estimated with recession sensors. The online thickness recession measurements are possible using intrusive break-wire sensors. In a break-wire arrangement, multiple pairs of wires are embedded in a TPS at different depths. The preparation of this type of sensor can be difficult and expensive, in particular because it is necessary to identify a suitable drilling technology (e.g. micro electrical discharge machining or laser drilling) for each ablative material thus to produce a series of blind holes at increasing depths from the face exposed to heat fluxes. Moreover, it is necessary to evaluate the quality of the produced sample by emission scanning electron microscope. Once the holes are drilled in the sample, the sensors must be inserted and glued using a high temperature adhesive, suitable for the ablative material subject to plasma testing. This method has been widely used for in-flight monitoring and requires embedded sensors and sophisticated analysis tools. The most recent one (i.e, recession sensor and ReGS) can be found in [42, 43] and reach sensitivities of tens of millimiters. This technique is very invasive since it determines heavy change in the test article geometry and shape that are not always acceptable.

The novel technique proposed in this work (widely discussed in the following sections) is based on the detection of γ-rays emitted by radioactive tracer. The technique has a high sensitivity (down to 0.1 μm) and is non-intrusive, since the γ-rays radioisotope tracer implantation does not change the mechanical and chemical features and the geometric shape of the tested material, and works also in a completely different wavelength range (of the order of tenths of picometers) compared to those involved in other techniques usually used for experimental characterization of hypersonic plasma and test article, i.e. LIF – Laser Induced Fluorescence, OES - Optical Emission Spectroscopy and IR cameras working in spectral

range that goes from UV to LW IR (Long Wavelength Infra Red). With these assumptions it is possible to assume that the interferences with respect to the signals coming from other methodologies as well as from the chemical-physical phenomena caused by the hot plasma-material interactions are reduced to the minimum and, moreover, having a high material penetrability there are no problems to guarantee access across the test chamber. Furthermore this real time, contactless technique has also the potential to be developed for in-flight TPS monitoring, positioning the γ detector in a specific position (e.g., behind the space vehicle aluminium or metallic alloys), thus significantly increasing the safety of the aerospace vehicles

- *CIRA Temperature and Wear rate novel methodologies*

With the goal to improve the experimental characterization capabilities over the test articles to be tested at CIRA hypersonic facility novel online, non-intrusive and more sensitive methodologies giving simultaneous informations both on the temperature and on the recession rate over the surface models, are under development at CIRA (the temperature uncertainty is less then 9 % and the recession rate sensitivity goes down to tens of μm). In particular quantitative two dimensional temperature maps can be obtained through dual color thermography [34, 44], while the recession rate can be obtained through ^{7}Be radioactive Surface ion beam Layer Implantation (SLI) [45-48]. The methodologies will be firstly tested on low and dense phenolic ablative materials such as cork-based composites [49] and SiO_2 based nanocomposites [50]. Moreover, the SLI will be also applied to reusable TPS such as UHTC and CMC composites. The novel techniques in the aerospace scenario are singularly described and the potential for a combined on-ground measurement is outline. On the basis of the results, future validation tests are planned, thanks to the use of the intense ^{7}Be radioactive beam available at the 3 MV Pelletron tandem accelerator of the CIRCE Laboratory and the GHIBLI plasma wind tunnel facility at CIRA.

2. Novel Temperature methodology using Dual Color infrared Thermography

Emissivity depends on temperature, wavelength, surface features of the target investigated. This parameter is unknown for innovative materials such as those employed for atmosphere reentry tested in PWT.

The thermal energy $\boldsymbol{E_{inc,\lambda}}$, that reaches the IR camera sensor at a specific wavelength λ, can be written [34]:

$$\boldsymbol{E_{inc,\lambda}}(\boldsymbol{\lambda}, \boldsymbol{\varepsilon_{obj}}, \boldsymbol{T_{obj}}) = \boldsymbol{\varepsilon_{obj,\lambda}}(\boldsymbol{\lambda}, \boldsymbol{T_{obj}})\boldsymbol{\tau_{atm}}\boldsymbol{E_{n,\lambda}}(\boldsymbol{\lambda}, \boldsymbol{T_{obj}}) + \left(\mathbf{1} - \boldsymbol{\varepsilon_{obj,\lambda}}(\boldsymbol{\lambda}, \boldsymbol{T_{obj}})\right)\boldsymbol{\tau_{atm}}\boldsymbol{E_{n,\lambda}}(\boldsymbol{\lambda},, \boldsymbol{T_{env}}) + (\mathbf{1} - \boldsymbol{\tau_{atm}})\boldsymbol{E_{n,\lambda}}(\boldsymbol{\lambda}, \boldsymbol{T_{atm}}) \quad (1)$$

where $\boldsymbol{\varepsilon_{obj,\lambda}}$ is the emissivity of the target at the wavelength $\boldsymbol{\lambda}$ at temperature $\boldsymbol{T_{obj}}$, $\boldsymbol{E_{n,\lambda}}$ is the monochromatic spectral black body emissive power, $\boldsymbol{T_{env}}$ is the environment temperature, $\boldsymbol{\tau_{atm}}$ is the atmosphere transmission coefficient, $\boldsymbol{E_{atm,\lambda}}$ is the spectral radiation emitted by the atmosphere at temperature $\boldsymbol{T_{atm}}$. Since the influence on the measurement of the atmosphere transmission is negligible, $\boldsymbol{\tau_{atm}}$ is considered equal to 1, besides when $\boldsymbol{T_{atm}} \ll \boldsymbol{T_{obj}}$ and $\boldsymbol{T_{env}} \ll \boldsymbol{T_{obj}}$, the 2nd and 3rd term in the second member of Eq.1 can be neglected.

Hence the ratio between thermal energy at two specific wavelengths can be written:

$$\boldsymbol{SR}(\boldsymbol{\lambda_i}, \boldsymbol{\lambda_j}, \boldsymbol{T_{obj}}) = \boldsymbol{\varepsilon_{\lambda_i}}\boldsymbol{E_{n,\lambda_i}}(\boldsymbol{T_{obj}}) \Big/ \boldsymbol{\varepsilon_{\lambda_j}}\boldsymbol{E_{n,\lambda_j}}(\boldsymbol{T_{obj}}) \quad (2)$$

and when the two working wavelengths are so close to keep valid the "grey body" hypothesis, the SR (Signal Ratio) becomes only a function of the temperature since the two emissivities at $\boldsymbol{\lambda_i}$ and $\boldsymbol{\lambda_j}$ wavelength can be elided, and the temperature can be obtained inverting Eq. 2.

The Ratio principle is already applied to the pyrometers with good results (dual color pyrometers) [51] but they can only give information about temperature on a specific target

spot. Application of this principle through thermography could give informations of two dimensional temperature maps free from emissivity rather than information on specific spot. Pyrometers work mainly with two adjacent detectors working at two adjacent wavelengths while thermal cameras use FPA (Focal Planar Array) that works in a wider infrared range. This means, for example, that a camera with a resolution of 640 x 380 pixel has about 24 x 10^4 detectors sensitive to the thermal radiation [52]. In this case the use of the radiation at two near wavelength can not consist to duplicate sensors in order to work at adjacent wavelength, but rather, it can consist to use internal wheel with narrow pass band filters working at adjacent wavelength [53]. So with this configuration, from the radiation emitted by the target ((1) see Fig.1) collected by the detector passing through the two filters ((2) and (3) see Fig.1), is possible to elide the emissivity through the ratio principle:

$$SR(T) = \frac{\varepsilon_1 \int_{\lambda_1}^{\lambda_2} R(\lambda,T) * F_1(\lambda) * P(\lambda,T) \delta\lambda}{\varepsilon_2 \int_{\lambda_1}^{\lambda_2} R(\lambda,T) * F_2(\lambda) * P(\lambda,T) \delta\lambda} \qquad (3)$$

where $R(\lambda, T)$ is the response curve of the IR camera detector, $F_1(\lambda)$ and $F_2(\lambda)$ the response curve of the two filters centered at λ_1 and λ_2 wavelength and with $P(\lambda, T)$ the analytical expression of Planck law.

Moreover this technique assumes that the temperature does not undergo variations when the wheel switches from one filter to the other and, under this assumption, it could be used for analysis in thermal stationary conditions. Today cameras with fast rotating wheel up to 100 Hz are available (ex., FLIR Orion 7600 [52]), in such a way that, when the observed phenomena does not chance in about 5 ms (the time required to acquire two opposite filtered signals, see next section), the temperature can be considered unchanged during non-stationary phenomena. Furthermore cameras usually work in LW (Long Wavelength) or MW (Medium Wavelength) spectral range, while pyrometers work in NIR (Near InfraRed) range. For this reason numerical analyses are needed in order to forecast uncertainties committed by

implementing this technique both for the cameras that works at different spectral ranges than pyrometers and that works with detectors characterized by different response curve (in terms of quantum efficiency) than the ones implemented in the pyrometers.

These techniques forecast the use of black bodies like Mikron M 305 (30 – 450 °C), M 310 (100 -1000 °C), M 390 (600 – 3000 °C) [34] to obtain the SR calibration curve (Signal Ratio collected by the detector though the two filters) as function of temperature, left part of Fig.2. The calibration curve (T_{dual} - red solid line in the right part of Fig.2) is used to associate the measured SR, during a test, to the temperature value. Of course since the grey body condition is an ideal condition, the ratio between emissivities at two working wavelength is not 1 and, as consequence, real temperature (T_{real} - blue dashed curve in the right part of Fig.2) can be different from the calibration curve.

2.1 Numerical tool: radiation and best filters determination

A numerical tool elaborated through Mathcad code has been developed and validated [34] at CIRA to provide an estimation of infrared radiation captured by the camera detector (RD, Eq. 4). A graphical scheme of the Eq. 4 is shown in Fig. 3: the radiation captured by the camera inserting the spectral emissivity trend of the target ε(λ,T), the detector response R(λ) and the filter response $F_1(\lambda)$ are coupled with planck law P(λ,T). This tool allows to define the best couple of filters and subsequently gives an accuracy estimation committed using the technique when the materials emissivity, that change with the wavelength, are taken into account (i.e. non grey body condition).

$$\boldsymbol{RD}(\lambda,T) = \int_{\lambda_1}^{\lambda_2} \varepsilon(\lambda,T) * R(\lambda) * F_1(\lambda) * P(\lambda,T)\delta\lambda \qquad (4)$$

In this paper, focused on the TPS Aerospace materials, the Orion 7600 camera has been used for different purposes.

The SR sensitivity increases by decreasing the filters central wavelengths and the FLIR Orion 7600 chosen camera works in MW spectral range (1.5-5.1 μm, lower part close to NIR). On the left side of Fig. 4, different trends of SR for different filter couples are shown in function of the temperature. The response curves of filters have been simulated with Gaussian functions and in particular the dashed dot purple curve presents a greater slope than the others and hence filters working at 2.0 and 2.1 μm represents the best combination in terms of SR sensitivity. However the filters choice was guided on what it was available on the market and the two SPECTROGON filters NB-2097-55 and NB-2210-47 [53], respectively centered at 2.097μm and 2.210 μm (right side of Fig.4) with a FWHM respectively of 55 nm and 47 nm, were chosen. More the SR varies with temperature more it can be associate to an unique temperature value, on the contrary, if the two wavelength are too close, the SR trend becomes too flat with temperature and a single temperature value becomes difficult due to the oscillation of the calibration curve related to the camera sensitivity [34]. On the other hand when the central filter wavelengths are too far, grey body hypothesis fail and ratio principle can not be used. The simulated SR calibration curve, obtained for the chosen couple of filters (2.1 and 2.2 μm), with a similar trend (slope: 2 x 10^{-4} /°C) to that in Fig. 9 in [34], is shown in Fig.5.

Furthermore, the FLIR Orion 7600 is equipped with an internal wheel able to rotate at high speed (up to 100 Hz) synchronized to the detector acquisition, allowing to work in non stationary conditions.

2.2 Experimental phase: feasibility analysis for a typical temperature trend in a hypersonic Plasma Wind Tunnel test campaign

Plasma Wind Tunnels testing campaigns are not frequently carried out, so one has to extract as much information as possible every time. Starting from an experimental temperature curve (black square marks in Fig. 6) obtained from an unknown and innovative UHTC coatings on CMC (Air Force Research Laboratory - AFRL) with a dual color pyrometer [54] technique, a trend at higher temperature conditions (up to 2500 °C) has been extrapolated. A particular attention has been paid to keep the original trend in terms of both the total duration of heating phase up to the maximum temperature value (in 115 s) and in terms of the slope. The following analytical law has been obtained (red circle points in Fig. 6):

$$T(t) = -1216\, e^{-\frac{t}{4}} - 1215\, e^{-\frac{t}{24}} + 2500 \quad (5)$$

This curve allows to consider temperatures in the range of 500 – 2500 °C covering the extremes heating conditions occurring in the reentry phase reproduced by the on-ground hypersonic facilities and it allows to make chance evaluation in 5 ms interval time (corresponding to the FLIR Orion 7600 time necessary to capture two adjacent frames).

As a matter of fact despite the wheel rotates with a frequency of 100 Hz, in order to guarantee the correct mechanical balance during the rotation and synchronization with the detector, the two filters are positioned in diametrically opposite positions, in such a way that half rotation necessary to acquire two adjacent frames occurs in 5 ms. In this time interval a change in temperature of 10^{-3} °C from the middle instant of the heating process up to the end of the test can be deduced, Eq.5, while a maximum variation of about 2 °C at 500° C (after 1.5 s the beginning of the trend). These variations are negligible in comparison with the absolute values and hence steady temperature can be considered for two adjacent frames. The ratio principle (Eq. 2) can be used in non stationary conditions during the typical hypersonic tests performed in PWT.

2.3 Dual Color indeterminations due to the non-grey body target behaviors

The most critical effort, to implement the dual color technique, however consists on the accuracy evaluation committed due the non grey body hypothesis at two adjacent working wavelengths.

Most common spectral emissivity material trend, found in literature [55], have been used to estimate the possible indeterminations committed through dual color technique due to non grey body condition, Fig.7. Difference between dual color simulated measurement (marks) and real trend (black solid line) are shown in left side of Fig.8.

Percentage errors between dual color (T_{dual}) and real (T_{real}) temperature values are defined as in the following:

$$Err = \frac{|T_{dual} - T_{real}|}{T_{real}} * 100 \quad (6)$$

The most significant results obtained are the following: the minimum and maximum uncertainty are obtained respectively with SiC (0.13 % at 2500°C) and C/SiC (9.3% at 2500°) materials. The curve with maximum error (C/SiC material) exibits a trend that increase with temperature, from a minimum of 3% at 500 °C to a maximum of 9.3% at 2500 °C (right side of Fig.8).

3. Novel Wear Rate methodology using Radioactive Tracers

Radioactive tracer techniques are nowadays routinely used for contactless, online wear and corrosion measurements, and representing an extremely powerful tool in material science and engineering [45, 46]. Indeed, they provide accurate and real-time data, allowing to monitor wear or corrosion without disassembly and physical inspection.

The new idea to implant radioactive ions (γ-ray emitters) into the TPS sample, can allow to obtain the evaluation of the recession thickness in a non-intrusive way, remotely and during the test, with higher accuracy respect to the measurements carried out until now in the

Aerospace field. To our knowledge, the measurement of instantaneous recession rate during plasma tests has never performed so far by means of radioactive implanted tracer in the material. The online measurement would provide interesting information about the ablation and erosion resistance of a material as the experimental conditions change (e.g. total enthalpy, values of heat flux and oxygen concentration) or at different surface temperatures reached during the experiment. The technique is more easily implemented for ablative materials, indeed we use this as a test case in the following. However, although UHTC and CMC are reusable TPSs, oxidation processes during reentry phase have also been observed [1]. Therefore the radioactive tracer techniques can be also adopted to evaluate recession rate in the case of reusable TPS materials, since the technical sensitivity can be really low, sub-micrometric (furthermore could be also used to implement monitoring techniques for PWT crucial components). Moreover this technique might later be developed to perform in-flight TPS monitoring, thus significantly increasing the safety of aerospace vehicles.

3.1 TPS recession rate simulation by γ-detection

The activity of the radioactive ions implanted in the TPS sample decreases when the wear depth reaches the tracer itself (ex., ^{7}Be) in the matter [47]. When the wear proceeds, the residual radioactivity of a sample marked with radiotracers provides information on the recession, within the uncertainty due to the knowledge of their depth distribution and the precision of the radioactivity measurement. The removed activity is transported away and not redistributed on the test sample both for the PWT facility pumping system and for the high speed of the plasma flow, giving a wind flux going from the nozzles, through the sample, to the diffuser (preliminary tests to verify the distribution of powders are planned using very low ^{7}Be activity). In order to investigate the feasibility of the proposed technique and identify the optimal condition for a test measurement, a full Monte Carlo simulation of a possible experimental setup was developed. In this simulation the residual activity on the TPS sample

wearing process is taken into account, to avoid the complicated, albeit potentially very informative, collection of the removed activity. The experimental set-up is simulated by means of Monte Carlo simulations carried out using the radioactive decay module available in GEANT4 toolkit [56], considering the detector in a realistic and close geometry in order to increase the detection efficiency. GEANT4 is a simulation environment for high-energy physics experiments, and widely used in aerospace science. It simulates all relevant physical processes taking place in matter along the passage of elementary particles interacting with ionizing radiation, that is tracked from the source to the detector. The code allows a relatively simple definition of complex volumes and of any configurations. The general particle source (GPS) module has been used as particle generator and the default physics list is used.

3.2 Detector materials and simulation code verifications

The present section aims to determine the dimensions of the $LaBr_3$(Ce) crystal specifications of γ -ray detector, to be then used in the recession rate simulations. Harsh environmental conditions play an important role, besides the usual detection parameters, i.e. as function of total, compton and photo-peak efficiencies for a given experimental geometry, and shielding materials as well as the amount of the ^{7}Be incorporation material. The simulation is focused on ^{7}Be since, as discussed in section 4, is the radioisotope used in the actual test. The ultimate goal is to minimize the amount of necessary ^{7}Be, and correspondingly relax the necessary radiation protection actions (that should be really few given the really low ^{7}Be radiation gamma and radiotoxicity constants), to achieve a desired precision in the determination of the recession rate. Special attention was devoted to the cerium-doped lanthanum crystals ($LaBr_3$(Ce)), that have gained popularity in gamma-ray spectroscopy due to the outstanding scintillation specifications, when compared to other scintillators. Indeed in comparison to thallium-doped sodium iodide (NaI(Tl)), often used as scintillation detector standards, $LaBr_3$(Ce) have better resolution by approximately a factor of 2 (3.5% vs 7% (FWHM) at 662

keV), a faster decay time (∼16 ns), which provides a time resolution of about 300 ps, a detection efficiency higher by a factor ∼1.3, thanks to the larger density of 5.29 (g/cm^3). Other very attractive features are the light output stability with respect to the operation temperature (negligible variation in the range -20 to +60 °C) and the stability of the energy resolution over a wide dynamic range of counting rate. The GEANT4 simulations of scintillator detectors have been already developed by the authors, and have been proven to reproduce experimental observations also in presence of complex geometries [57, 58]. Moreover as a preliminary step for the simulation of the final experimental setup, all materials (the crystal, the crystal housing and the sample holder (slab)) and the geometry used in the GEANT4 code were included in a very simple configuration, including an isotropic ^{7}Be point source of 3 MBq and the results have been compared with literature values:

- **GEANT4 code:** The simulated total efficiency results, obtained for a NaI(TI) crystal of 2x2 inch, has been of 2.96±0.03 % and 2.59±0.03 % for energies of respectively 478 and 662 keV at a distance (d) between the crystal and the source of 50 mm [59]. In addition, the peak-to-total efficiency value of 0.58±0.02 at energy of 478 keV for d=100 mm [60] was also determined. Both results are in agreement with literature values [59, 60].

- **$LaBr_3$(Ce) Material:** The photo-peak efficiency for a $LaBr_3$(Ce) crystal of 2x2 inch was 1.28±0.04, which is ∼1.3 times the value that would have been obtained with the NaI(TI) crystal, as indicated by the ORTEC specifications [61] at energy of 662 keV and d=50 mm.

- **Geometry:** The photo-peak efficiency scales with solid angle $\Omega = A/d^2$ (for d >> a) where ”a” is the radius of the cylindrical crystal surface A [60]. The started simulated geometrical configuration was: 2x2 inch NaI(TI) crystal and d= 300 mm.

- **Shielding attenuation coefficient:** The reduction of the γ-rays impinging onto the crystal for the presence of the TPS slab, on the left down side of Fig. 9, has been verified comparing the simulation results to the attenuation law for rays in terms of the mass attenuation coefficient (μ/ρ= linear attenuation coefficient/density of the medium) [60]. An Al (Aluminum) or Fe (Iron) material was used (100 mm x 100 mm x 1 mm (height x width x depth)) and positioned between the point source and the crystal. The $LaBr_3$(Ce) 2x2 inch crystal photo-peak efficiency simulation, performed at d= 50 mm and for different plate positions (between 1 and 49 mm) from the ^{7}Be point source, has shown an average value of 1.99±0.01 % and 1.92±0.02 % respectively for Al and Fe. The attenuation law obtained respectively with μ/ρ= 0.085 and 0.088 cm^2/g with ρ= 2.699 and 7.874 g/cm^3, results in 2.00 % and 1.91 % for Al and Fe [62].

In a second step, the full experimental set up, shown in the right panel of Fig.9, was simulated. In Figure 10, the total, compton and photo-peak efficiencies as a function of the $LaBr_3$(Ce) crystal dimensions, are shown. A 2x2 inch crystal on experiment constrains, small enough to be used in the test article support, and on desired efficiency bases was chosen. An ablative sample, made of about 25% of filler and 75% of phenolic resin (C_7H_6O) [50] of a dimensions of 30 mm x 30 mm x 25 mm (height x width x depth) was installed in front of the detector. In the sample, at a depth of 7.5 mm 3MBq of ^{7}Be were supposed to be implanted, with a uniform distribution over a rectangular area of 30 mm x 16 mm (height x depth). The center of the rectangular strip is at 54.5 mm from the $LaBr_3$(Ce) crystal. The minimum distance between the detector and the sample holder was 35 mm. The total, compton and photo-peak efficiencies for this experiment configurations are respectively 3.06±0.03 % and 1.46±0.03 %. These efficiencies are slightly reduced by 1 mm Al sample holder and the 1.5 mm Al crystal housing down to respectively 3.00 % and 1.41 %.

3.3 Gamma rays for TPS recession rate

The results of the TPS recession rate simulations and the accuracy of the method is extensively discussed in an accompanying papers [48]. Briefly, on the base of geometric and efficiencies considerations, a cylindrical 2x2 inch LaBr3(Ce) crystal, whose characteristics have been inserted according to actual manufacturer specifications, has been chosen. Since the γ-rays flux is appreciably attenuated by the sample holder and crystal housing these are included in the simulation. The simulation was designed to study a realistic customer request regarding an ablative sample of 80 mm long that does not wear more than 20% of its thickness in 120 seconds that, assuming a constant wear rate, corresponds to a recession rate of about 0.13 mm/s, see Table 1 [63]. The GEANT4 simulations were carried out for large number of events, assuming a uniformly distributed rectangular source as mentioned previously. For each ^{7}Be decay event with a γ-ray energy of 478 keV, the energy deposited in the detector has been simulated and the photo-peak output files in ASCII format were generated. A recession rate simulation results, where was supposed a γ-ray collection time of 3.75 s, is also shown in the right side of Fig. 12 (blue diamond marks). On the base of simulation it was also found that if the activity A_0 has a uniform depth distribution, over a rectangular area of 3 x 16 (height x depth) mm^2 starting at sample's surface that has a distance r from the crystal front face between R_{max} = 62.5 mm and R_{min} = 46.5 mm, the wear of the sample at a rate ρ corresponds to a variation of the activity as

$$\boldsymbol{A(t) = A_0}\left(\mathbf{1} - \frac{\rho}{R_{min}-R_{max}}t\right) \quad (7)$$

taking into account that in first approximation the detector efficiency ε varies as S/r^2, with S the area of the front face of the crystal. The expected number of γ-rays detected by the crystal in an interval Δt at the time t is given by:

$$\frac{\boldsymbol{N(t)}}{\boldsymbol{A_0}} = \boldsymbol{B_r}\frac{\boldsymbol{S}}{\boldsymbol{R_{max}-R_{min}}}\left(\frac{\mathbf{1}}{\boldsymbol{R_{min}}} - \frac{1}{R_{max}-\rho t}\right)\Delta t \quad (8)$$

a function having only the recession rate ρ as unknown parameter. Measurements of the TPS wear speed by means of radioactive tracer through beam implantation are possible, and to determine the shape in time of the recession at about 0.13 mm/s, with a sensitivity of 0.5 mm and a precision and accuracy respectively of about 10% and 1%, an incorporated activity of about 10 kBq should be used. It is worth to underline that the results depend on the supposed experimental arrangement, in particular on the assumed activity needed and on its distribution on the sample and the measurement time, that can be tailored in order to obtain the desired precision and accuracy.

4. Method and Applications

If for the dual color measurements is necessary to choose the right infrared camera and filtes and calibrate it through black bodies, a key requirement for wear measurements using radioactive tracers is the accurate knowledge of their density distribution, in order to infer the wear parameters from the observed variations of radioactivity. The Surface Layer Implantation (SLI), briefly described in the following, using a radioactive ion beam seems the most suitable for the TPS aerospace applications. Radioactive ion beam implantation can minimize the impact of the necessary incorporation of radiotracers and it allows to tailor the depth profile, thus allowing sub-millimetric (for ablative materials) as well as sub-micrometric (for ceramic UHTCs, CMCs) wear measurements. We present here a possible study for a test measurement using the ^{7}Be ion beam available at CIRCE and the GHIBLI plasma wind tunnel at CIRA, to investigate the feasibility of the proposed methods. The validation of the techniques will be performed by comparison to plasma testing on ablative samples and the experimental phase will be focused on the determination of the temperature and the recession rate, obtained measuring the residual activity on the sample while undergoes ablation effects by means of high heat fluxes. As matter of fact the validation of the

techniques will be performed by means of GHIBLI, briefly discussed in the following, on commercial ablative samples.

4.1 Surface Layer Implantation techniques

The radioactive tracer techniques historically used for material science and engineering are: BA (Bulk activation) and SLA (Surface Layer Activation). In both cases, radio-isotopes are produced directly in the sample by irradiating it with neutrons, for BA, or light charged particles (protons, deuterons and alphas), for SLA. However, the utilization of a pure RII (Radioactive Ion Implantation) [64, 65] beam as tracer offers a wider range of applicability and a higher sensitivity, since the implantation can be done in whatever material, and the implantation damage induced by the beam is drastically reduced, not including the effect of the low activation cross section. In this approach a RIB (Radioactive Ion Beam) is used to implant radio isotopes in the surface layer of the sample. The implantation depth is determined by the beam energy and the stopping power of the radioactive ion in the sample: therefore a proper modulation of the ion beam energy during the implantation in a given material allows to tailor the radio isotope depth distributions. The drastic reduction of the radiation damage (up to a factor 10^6) in comparison with SLA allows application of RII in principle to any material, therefore providing a powerful tool for comparative studies. The main problem of this technique is the availability of a suitable RIB. The half lives of the chosen radioisotope should be as short as possible, but not too much to allow an easy handling, The best compromise should be found in order to minimize the amount of activity needed to achieve the required sensitivity. ^{7}Be is a good candidate for the experiments. It decays by electron capture to ^{7}Li, with a probability of about 10 % of emitting γ-ray (E_γ= 478 keV), corresponding to the population of the first excited state in ^{7}Li. The details of the procedure followed to produce the ^{7}Be beam are described elsewhere [47, 66, 67]. Briefly the ^{7}Be nuclides are formed via the ^{7}Li(p,n)^{7}Be reaction in an external cyclotron. The ^{7}Be

cathodes are processed at the Isotopic Laboratory at CIRCE, where the ^{7}Be nuclides are extracted from the ^{7}Li bulk. The preparation takes place in a hood shielded with 10 cm of lead to protect the operator. Up to 99 % of the activity is collected in a liquid solution, while ^{7}Li is depleted by about six orders of magnitude. Thus the solution which is dropped in copper cathodes still contains about equal amounts of ^{7}Li and ^{7}Be. The activities of the ^{7}Be cathodes can be up to to several GBq, making possible the implantation of several MBq as required by the recession rate simulations. This amount of activity, together with the low radio-toxicity of ^{7}Be, due to its decay mode, makes it easy to fulfill the radioprotection requirements and obtain the necessary permissions. The ^{7}Be cathodes are finally installed into a dedicated Cs sputtering source at the CIRCE laboratory and then "shoot" in the TPS sample that will be tested in the GHIBLI plasma wind tunnel.

4.1.1 CIRCE accelerator

The +3 MV CIRCE [68, 69] tandem accelerator will be used to produce the activated TPS samples. The CIRCE accelerator originally equipped for radiocarbon, was upgraded both to perform AMS (Accelerator Mass Spectrometry) with actinides (^{236}U, ^{239}Pu and its isotopes) ions [70-72] for environmental measurements [73-76], thus having the possibility of generating ion beam in the entire periodic table, and to produce and transport a high intensity RIB.

Briefly the negative ions, are accelerated at energies of several tens of keV range (e.g. ^{7}Be^{16}O^{-} at 67 keV) and are energy and mass selected by the first ± 45° spherical electrostatic analyzer and the 90° double focusing LE (Low Energy) injector magnet. The LE insulated stainless steel chamber can be biased up to 15 kV for beam sequencing. The accelerator is contained inside a vessel filled with sulfur hexafluoride (SF_6) at a pressure of about 6 bar and so the Terminal Voltage can be kept constant up to 3.000 MV. At the terminal, where molecular ions are broken, the ions loose electrons in the Argon stripper. The gas is

recirculated by two turbo-pumps and the working pressure is about 6.0 mTorr for $^{7}Be^{x+}$ at terminal voltage needed for the specific application. The ions are then post stripped to 4+ charge state and then selected with the 90° hight energy magnet and the 45° electrostatic spherical analyzers and implanted in the TPS sample where the γ-rays are counted with an appropriate detector.

4.2 GHIBLI Plasma Wind Tunnel

In order to perform the plasma testing for the TPS recession rate experiments, the GHIBLI facility at CIRA, Fig. 11, will be used. In the following a brief description on the GHIBLI system [77] is given. It is a hypersonic plasma wind tunnel, where the hot flow is generated in a 2 MW segmented arc heater running with Nitrogen and Air (ranges: 2.5-25 MJ/Kg for the total enthalpy and 8-10 Mach for the velocity).

Inside the arc heater column, the subsonic plasma flows, goes to the convergent-divergent nozzle where it is accelerated to hypersonic speed. In the test chamber the interaction of plasma with the TPS sample occurs, then the flow is conveyed in a diffuser pick-up for the pressure recovery. Hence, a heat exchanger reduces the high temperature of the flow and a vacuum system provides the proper suction power, during the facility operation, before the controlled ejection of the flow into the free atmosphere. The GHIBLI facility is able to simulate the reentry conditions into Earths atmosphere of the space vehicles. It allows aerothermodynamic testing in high enthalpy hypersonic flow (maximum 60 g/s) conditions of maximum 80-mm diameter models. Due to its own characteristics, it is well suited in the frame of projects for the development of new metodology, as well as to the development, selection, qualification and acceptance of high temperature materials.

5. Summary and Outlooks

The Dual Color Infrared methodology (allowing to obtain two dimensional free emissivity temperature maps) and the Recession Rate using radioactive tracers are two Novel Techniques, still in develop at CIRA, and able to give a contactless, online, high sensitivity temperature and wear informations, over also N spots, on the TPS materials under on-ground PWT tests (Fig. 12). The former might later be developed to perform in-flight TPS monitoring, thus significantly increasing the safety of the aerospace vehicles.

A uncertainty, between real and dual color measured temperature, lower than 1% has been revealed for SiC, while about 9% was associated to C/SiC. This technique can be really useful when materials tested in Plasma Wind Tunnel are innovative and their features are unknown in terms of emissivity spectral behavior. Besides chemical and mechanical material features due to the hypersonic flows, significantly change are due to the chemical interaction between plasma species and materials itself. It has been shown that measurements of the TPS wear speed (recession rate) by means of radioactive tracer through beam implantation are possible, and to determine the shape in time of the recession, at about 0.13 mm/s (a tipical wearing for re-entry phase, tab. 1), an incorporated activity of about 10 kBq should be used.

On the basis of the results, possible experimental validation tests are planned, thanks to the use of the intense ^{7}Be radioactive beam available at the 3 MV Pelletron tandem accelerator of the CIRCE Laboratory and the GHIBLI plasma wind tunnel facility at CIRA. The experimental phase will be guided by three basic steps of Design, Qualification and Verification:

1. Simulations of the thermal flux, temperature and recession rates by CFD and Thermo-structural analysis.

2. Manufacturing of test article and experiment itself: The validation will be performed by plasma testing on ablative test article and the experimental phase will be focused on the determination of the temperature and the recession rate.

3. Verification and rebuilding of simulations and modelling performed: The goal of the activity is to set the bases to develop a remote, on-line, high sensitivity and non-intrusive metodology that allows to have simultaneously temperature and wear aerospace material informations, to control in real time the status as well as to compare the experimental results with simulations and to validate a numerical model

that could be employed in future analyses to predict the failure of a generic structural component.

Acknowledgements

This work was supported by CIRA – Metodologie Fisiche Innovative per l'Aerospazio (MEFIA) - project through the PRogramma Nazionale di Ricerche Aerospaziali (PRORA).

REFERENCES

[1] W. G. Fahrenholtz, E. J. Wuchina, W. E. Lee, Y. Zhou, Ultra-High Temperature Ceramics: Materials for Extreme Environment Applications, Wiley - The American Ceramic Society, ISBN: 978-1-118-70078-5 (2014) 1-441.

[2] T. Laux, T. Ullmann, M. Auweter-Kurtz, H. Hald, A. Kurz, Investigation of thermal protection materials along an X-38 re-entry trajectory by plasma wind tunnel simulations, 2nd International Symposium on Atmospheric Reentry Vehicles and Systems - Proceedings of the Association Aronautique et Astronautique de France, (2001) 1-9.

[3] D.E. Glass, Ceramic matrix composite (CMC) thermal protection systems (TPS) and hot structures for hypersonic vehicles, 15nd AIAA Space Planes and Hypersonic Systems and Technologies Conference, AIAA-2008-2682 (2008) 1-36.

[4] D. Alfano, Spectroscopic Properties of Carbon Fibre Reinforced Silicon Carbide Composites for Aerospace Applications, Properties and Applications of Silicon Carbide. In Tech, 2011.

[5] G. Tumino, S. Mancuso, J.-M. Gallego, S. Dussy, J.-P. Preaud, G. Di Vita and P. Brunner, Acta Astronautica, 124 (2016) 2-17.

[6] W. Krenkel, Ceramic Matrix Composites: Fiber Reinforced Ceramics and their Applications, Wiley - The American Ceramic Society, ISBN: 978-3-527-31361-7 (2008) 1-418.

[7] S. D. Williams and D. M. Curry, Assessing the orbiter thermal environment using flight data, J. Spacecraft and Rockets, 21 (1984) 534-541.

[8] W. G. Fahrenholtz, G. E. Hilmas, I. G. Talmy, J. A. Zaykoski, Refractory Diborides of Zirconium and Hafnium, Journal of the American Ceramic Society 90 (2007) 1347-1364.

[9] A. Chamberlain, W. Fahrenholtz, G. Hilmas, D. Ellerby, Oxidation of ZrB_2-SiC Ceramic under Atmospheric and Reentry Conditions, Refractories Applications Transactions 1 (2005) 1-8.

[10] J. Marschall, D. A. Pejakovic, W.G. Fahrenholtz, G.E. Hilmas, F. Panerai, O. Chazot, Temperature Jump Phenomenon During Plasmatron Testing of ZrB_2-SiC Ultrahigh-Temperature Ceramics, J. Thermophys. Heat Transfer 26 (2012) 559-572.

[11] M. Balat-Pichelin, L. Charpentier, F. Panerai, O. Chazot, B. Helber, K. Nickel, Passive/active oxidation transition for CMC structural materials designed for the IXV vehicle re-entry phase, Journal of the European Ceramic Society, 35 (2015) 487-502.

[12] F. Panerai, B. Helber, O. Chazot, M. Balat-Pichelin, Surface temperature jump beyond active oxidation of carbon/silicon carbide composites in extreme aerothermal conditions, Carbon, 71 (2014) 102-119.

[13] M. Balat-Pichelin, Determination of the active-to-passive transition in the oxidation of silicon carbide in standard and microwave-excited air, Journal of the European Ceramic Society, 16 (1996) 55-62.

[14] J. E. Pavlosky, G. St. Leger, Apollo experience report - Thermal protection subsystem, NASA technical note, NASA TN D-7564 (1974) 1-24.

[15] G. W. Sutton, The initial development of ablation heat protection: An historical perspective, J. Spacecraft and Rockets, 19(1) (1982) 3-11.

[16] P. J. Schneider, T. A. Dolton, G. W. Reed, Mechanical erosion of charring ablators in ground test and re-entry environments, AIAA Journal, 6(1) (1968) 64-72.

[17] J. M. Bouilly, F. Bonnefond, L. Dariol, P. Jullien, F. Leleu. Ablative thermal protection systems for entry in Mars atmosphere. A presentation of materials solutions and testing capabilities. 4th International planetary probe workshop, 2006.

[18] G. S. Rufolo, F. Camarri, R. Romano, D. Vernani, G. Tumino, The Intermediate Experimental Vehicle in flight experimentation from the design to the flight. 8th European Conference on Aerothermodynamics for Space Vehicles, 2015 Lisbon, Portugal.

[19] H. K. Tran, Development of Lightweight Ceramic Ablators and Arc-Jet Test Results, Technical Memorandum TM-108798, NASA Ames Research Center (1994) 1-25.

[20] H. K. Tran et al., Phenolic Impregnated Carbon Ablators (PICA) as Thermal Protection Systems for Discovery Missions, Technical Memorandum TM 110440, NASA Ames Research Center (1997) 1-72.

[21] D. A. Kontinos, M. J. Wright, Introduction: Atmospheric Entry of the Stardust Sample Return Capsule, J. Spacecraft and Rockets 47 (2010) 705-707.

[22] F. S. Milos, Y. K. Chen, Ablation and Thermal Response Property Model Validation for Phenolic Impregnated Carbon Ablator, J. Spacecraft and Rockets 47 (2010) 786-805.

[23] F. S. Milos, Y. K. Chen, T. Gökçen, Nonequilibrium Ablation of Phenolic Impregnated Carbon Ablator, J. Spacecraft and Rockets 49 (2012) 894-904.

[24] Ph. Tran, J. C. Paulat, P. Boukhobza, Re-entry flight experiments lessons learned – The Atmospheric Reentry Demonstrator ARD, RTO-EN-AVT-130 (2007) 1-46.

[25] A. Scott, S. A. Berry, T. J. Horvath, R. P. Lillard, B. S. Kirk, A. M. Cassady, Aerothermal testing for project orion crew exploration vehicle, 41st AIAA Thermophysics Conference, AIAA paper 2009-3842, 2009.

[26] J. M. Bouilly, S. His, J. L. Macret, The ARD thermal protection system, 1st International symposium on ARVS, 2003.

[27] I. Şakraker, B. Helber, O. Chazot, Experimental characterization of cork based thermal protection material P50. 8th European Symposium on Aerothermodynamics for Space Vehicles, March 2015, Lisbon, Portugal.

[28] G.W. Sutton, The initial development of ablation heat protection: An historical perspective, J. Spacecraft and Rockets 19(1) (1982) 3-11.

[29] F.S. Milos, D. J. Rasky, Review of numerical procedures for computational surface thermochemistry, Journal of Thermophysics and Heat Transfer, 8(1) (1994) 24-34.

[30] B. Müller, U. Renz, S. Hoppe, F. Klocke, Radiation thermometry at a high-speed turning process, Journal of Manufacturing Science and Engineering 126 (2004) 488-495.

[31] G. Machin et al., The European project on high temperature measurement solutions in industry (HiTeMS) – A summary of achievements, Measurement 78 (2016) 168-179.

[32] C. Zhang et al., Surface temperature measurement of the plasma facing components with the Multi-Spectral Infrared thermography diagnostics in Tokamaks, Infrared Physics & Technology (2017).

[33] K.-P. Möllmann, F. Pinno, M. Vollmer, Two-color or ratio thermal imaging – potentials and limits, InfraMation 2010 Proceedings.

[34] L. Savino, M. De Cesare, M. Musto, G. Rotondo, F, De Filippis, A. Del Vecchio, F. Russo, Free emissivity temperature investigations by dual color applied physics methodology in the mid- and long- infrared ranges, International Journal of Thermal Sciences 117 (2017) 328-341.

[35] B. Helber, A. Turchi, J. B. Scoggins, A. Hubin, T. E. Magin, Experimental investigation of ablation pyrolysis processes of carbon-phenolic ablators in atmospheric entry plasmas, International Journal of Heat an Mass Transfer 100 (2016) 810-824.

[36] B. Helber, O. Chazot, A. Hubin, T. E. Magin, Microstructure and gas-surface interaction studies of a low-density carbon-bonded carbon fiber composite in atmospheric entry plasma, Composites part A 72 (2015) 96-107.

[37] E. T. Schairer and J. T. Heineck, Photogrammetric Recession Measurements of Ablative Materials in Arcjets, Measurement Science and Technology 21 (2010) 025304 (15pp).

[38] S. Loehle, T. Staebler, T. Reimer, A. Cefalu, Photogrammetric Surface Analysis of Ablation Processes in High-Enthalpy Air Plasma Flow, AIAA JOURNAL 53 (2015) 3187-. 3195.

[39] P. Sherrouse, D. Carver, Demonstated Real-Time Recession Measurements of Flat Materials During Testing in High-Enthalpy Flows, 30th Aerospace Sciences Meeting & Exhibit, 6-9 January 1992, Reno NV, AIAA-92-0765.

[40] A. S. Pagan et al., Laser-based surface recession measurements of ablating heat shield materials in high-enthalpy flows, 8th European Symposium on Aerothermodynamics for Space Vehicles 2 – 6 March 2015, Lisbon, Portugal.

[41] B. D. Butler, M. Winter, M. Stackpoole, Characterization of Virgin and Charred PICA Seeded for Remote Recession Measurements, AIAA AVIATION Forum, 47th AIAA Thermophysics Conference, 5-9 June 2017, Denver - Colorado, AIAA 2017-3357.

[42] B. Massuti-Ballaster, A. S. Pagan, G. Herdrich, G. Vekinis, A. Marinou, Ch. Zuber, H. Ritter, Experimental evaluation of an in-flight surface recession sensor for ablative thermal protection systems, IPPW-14, 2017.

[43] G. Vekinis, A. Marinou, Reconstructing TPS recession using the ReGS sensor, IPPW-14 2017.

[44] M. Musto, G. Rotondo, M. De Cesare, A. Del Vecchio, L. Savino, F. De Filippis, Error analysis on measurement temperature by means Dual-Color Thermography Technique, Measurement 90 (2016) 265-277.

[45] G. Jones, Multiple Location Radioactive Wear Analysis Techniques, SAE Technical Paper 790872 (1979), https://doi.org/10.4271/790872.

[46] F. Ditroi and I. Mahunka, Thin layer activation of non-metallic materials by using nuclear implantation, Nucl. Instr. Meth. Phys. Res. B, 113 (1996) 415-419.

[47] B.N. Limata, L. Gialanella, A. Di Leva, N. De Cesare, A. D'Onofrio, G. Gyurky, C. Rolfs, M. Romano, D. Rogalla, C. Rossi, M. Russo, E. Somorjai, F. Terrasi, ^{7}Be radioactive beam production at CIRCE and its utilization in basic and applied physics, Nucl. Instr. Meth. Phys. Res. B, 266 (2008) 2117.

[48] M. De Cesare, A. Di Leva, A. Del Vecchio, L. Gialanella, A novel recession rate physics methodology for space applications at CIRA by means of CIRCE radioactive beam tracers, J. Phys. D: Appl. Phys. 51 (2018) 09LT01

[49] G. Pinaud, A. J. van Eekelen, J. M. Bouilly, Aerofast: development of cork TPS material and a 3D comparative thermal/ablation analysis of an Apollo & a biconic sled shape for an aerocapture mission, 8th International Probe Workshop (2011).

[50] M. De Stefano Fumo, R. Gardi, M. Belardo, D. Alfano, G. Marino, S. Cantoni, Status of CIRA Research and Development Activities on TPS&HS for Space Transportation Systems. 8th European Workshop on TPS & HS, Noordwijck Netherland, 19-22 April, 2016.

[51] C. Purpura, E. Trifoni, D. Alfano, G. Cosentino, Materials surface emissivity analyses performed by the combined use of dual and single color optical pyrometers, Proceedings of the International Astronautical Congress – IAC, 8 (2013) 6174-6181.

[52] FLIR web site: http://www.flir.com

[53] Spectrogon web site: http://www.spectrogon.com

[54] C. Purpua, E. Trifoni, A. Martucci, M. De Stefano Fumo, C. Carney, D. King, M. Cinibulk, Experimental Investigation of the Emissivity of UHTC Coatings on CMC Materials in GHIBLI Plasma Wind Tunnel Tests, 68th International Astronautical Congress (Adelaide – Australia) 25-29/09 (2017).

[55] G. Neuer, Spectral and total emissivity measurements of highly emitting materials, Int. J. Thermophys. 16(1) (1995) 257-265.

[56] S. Agostinelli et al., Geant4-a simulation toolkit, Nucl. Instr. Meth. Phys. Res. A, 506 (2003) 250-303.

[57] A. Di Leva, M. De Cesare, D. Schurmann, N. De Cesare, A. D'Onofrio, L. Gialanella, R. Kunz, G. Imbriani, A. Ordine, V. Roca, D. Rogalla, C. Rolfs, M. Romano, E. Somorjai, F. Strieder, F. Terrasi, Recoil separator ERNA: Measurement of $^{3}He(\alpha,\gamma)^{7}Be$, Nucl. Instr. Meth. Phys. Res. A, 595 (2008) 381-390.

[58] D. Schurmann, A. Di Leva, L. Gialanella, R. Kunz, F. Strieder, N. De Cesare, M. De Cesare, A. D'Onofriob, K. Fortaka, G. Imbriani, D. Rogalla, M. Romano, F. Terrasi, Study of the 6.05 MeV cascade transition in $^{12}C(\alpha,\gamma)^{16}O$, Phys. Let. B, 703 (2011) 557561.

[59] B.J. Snyder, Tabulated efficiencies of some well-type gamma ray scintillation detectors for various geometries, Nucl. Instr. and Meth. Phys. Res. A 53 (1967) 313-319.

[60] G.F. Knoll, Radiation Detection and Measuremet Book, 3rd ed. ISBN 0-471-07338-5 (2000).

[61] Lanthanum Bromide Scintillation Detectors - ORTEC web site: http://www.ortec-online.com/

[62] J.W. Allison, Gamma-radiation Absorption Coeffcients of Various Materials allowing for Bremstrahlung and other Secondary Radiations, Aust. J. Phys. (Provided by NASA Astrophysics Data System) 14 (1967) 443

[63] ABLAMOD (Advanced aBLAtion characterization and MODelling), EUROPEAN COMMISSION PROJECT, 2013-2015: http://cordis.europa.eu/project/rcn/106604_en.html

[64] Wm. M. Harris, R. Ronningen, H. Schock, R. Schalek, D. Grummon, Radioactive ion implantation for wear studies, Nucl. Instrum. Methods Phys. Res., Sect. A 353, 583 (1994).

[65] P. Fehsenfeld, C. Eifrig, R.Kubat, Application of RNB for high sensitive wear diagnostics in medicine technique and industry, Nucl. Phys. A 701, 235c (2002).

[66] L. Gialanella at al., Off-line production of a 7Be radioactive ion beam, Nucl. Instr. Meth. Phys. Res. B, 197 (2002) 150-154.

[67] L. Gialanella et al., Wear Measurements By Means Of Radioactive Ion Implantation, Application of Accelerators in Research and Industry, AIP Conf. Proc., 680 (2003) 469-473.

[68] M. De Cesare, N. De Cesare, A. D'Onofrio, L.K. Fifield, L. Gialanella, F. Terrasi, Mass and abundance ^{236}U sensitivities at CIRCE, Nucl. Instr. Meth. Phys. Res. B, 361 (2015) 483-487.

[69] M. De Cesare, N. De Cesare, A. D'Onofrio, L.K. Fifield, L. Gialanella, F. Terrasi, Uranium beam characterization at CIRCE for background and contamination determinations, Appl. Radiat. Isotopes, 103 (2015) 166-172.

[70] M. De Cesare et al., Actinides AMS at CIRCE and ^{236}U and Pu measurements of structural and environmental samples from in and around a mothballed nuclear power plant, Nucl. Instr. Meth. Phys. Res. B, 294 (2013) 152-159.

[71] M. De Cesare, Y. Guan, F. Quinto, C. Sabbarese, N. De Cesare, A. D'Onofrio, L. Gialanella, A. Petraglia, V. Roca, F. Terrasi, Optimization of ^{236}U AMS at CIRCE, Radiocarbon, 52 (2010) 286-294.

[72] Y.-J. Guan, M. De Cesare, F. Terrasi, F. Quinto, C. Sabbarese, N. De Cesare, A. D'Onofrio, H.-J. Wang, ^{236}U AMS measurement at CIRCE, Chinese Physics C, 34 (2010) 1729-1732.

[73] M. De Cesare, L.K. Fifield , S.G. Tims, Uranium comparison by means of AMS and ICP-MS and Pu and ^{137}Cs results around an Italian nuclear power plant, EPJ Web of Conference, 91 (2015) 0004, 1-5.

[74] A. Petraglia, C. Sabbarese, M. De Cesare, N. De Cesare, F. Quinto, F. Terrasi, A. D'Onofrio, P. Steier, L.K. Fifield, A. M. Esposito, Assessment of the radiological impact of a decommissioned nuclear power plant in Italy, Radioprotection, 47(2) (2012) 285-297.

[75] S. G. Tims, M. Srncik, L.K. Fifield, A. Wallner, M. De Cesare, Journal of Environmental Radioactivity, 151 (2016) 563-567.

[76] M. Srncik, S.G. Tims, M. De Cesare, L.K. Fifield, Journal of Environmental Radioactivity 132 (2014) 108-114.

[77] C. Purpura, F. De Filippis, E. Graps, E. Trifoni, R. Savino, The GHIBLI plasma wind tunnel: Description of the new CIRA-PWT facility, Acta Astronautica, 61 (2007) 331-340.

Table 1. In the table measured ablative Recession Rate at different heat flux values for three different materials (Carbon Phenolic, Cork Based, Silicon Based) are shown. A mean value, for the heat flux in a range of 0.8 - 2 MW/m^2, corresponds to a mean recession rate of about 0.13 mm/s (16 mm in 120 s).

Material	**Flux** **MW/m^2**	**Recession Rate** **mm/s**
Carbon Phenolic	0.86	0.08
	1.24	0.10
	2.00	0.17
	10.00	0.38
Cork based	0.84	0.07
	1.20	0.08
	2.00	0.14
Silicon based	0.86	0.05
	1.24	0.08
	2.00	0.19

Figure captions

Figure 1. Dual color ratio scheme applied to the thermography, see text, is shown.

Figure 2. Thermocamera and black body on the left, SR calibration curve in dual color technique on the right are shown, see text.

Figure 3. Graphical representation of radiation detected by the Infrared camera expressed in Eq. 4 is shown, see text.

Figure 4. On the left side the SR trend in function of the temperature for different couples of filters is shown as well as, on the right, the Gaussians response curves representative of the best filters combination (2.1 and 2.2 μm), see text.

Figure 5. SR trend in function of the temperature for the 2.1 and 2.2 μm best filter combination is shown. The uncertainty curves due to the camera sensitivity and black body stability are superimposed, in the present scale, to the SR one.

Figure 6. It is shown a typical Trend of temperature, measured with two color pyrometer, over a spot on a target subjected to hypersonic jet (curve in black [1]). The curve with circular marks represent numerically the trend of temperature with time at most critical condition in terms of heat flux taking into account features of the square marks curve in terms of slope and total duration, see text.

Figure 7. Typical Trend of emissivity with wavelength for materials found in literature with features similar to the ones used in hypersonic tests. Dot for SiC, dashed for Graphite and solid line for C/SiC.

Figure 8. On the left side, temperature trend obtained with the dual color technique for the materials in Fig. 7 and, on the right, the dual color temperature trend in function of time for C/SiC material including error bars are shown, see text.

Figure 9. On the left upper side, the 2x2 inch cylindric $LaBr_3$(Ce) crystal and the isotropic ^{7}Be point source of 100 Bq (as an example) are shown. On the left down side a 1.5 mm Al thick crystal housing and 1 mm Al thick sample holder (slab) of 100 mm x 100 mm x 1 mm (height x width x depth) have been introduced, see text. On the right upper side a schematic layout of the experimental set up, for the starting efficiency of the recession rate simulations, is also shown. Besides the 1.5 mm Al thick crystal housing and 1 mm Al thick salb, the 2x2 inch cylindric $LaBr_3$(Ce) crystal and the 30 mm x 30 mm x 25 mm (height x width x depth) ablative sample distant 37.5 mm are also shown. In the right down side, the crystal and the ablative sample, are rotated clockwise of 90°. A 100 Bq of ^{7}Be is incorporated (as an example), see text.

Figure 10. Cylindric $LaBr_3$(Ce) detection efficiency as function of the crystal dimensions (cylinder radius x depth) at 54.5 mm from the ^{7}Be implantation center (right side of Fig.9). Blue diamonds indicate the photo-peak efficiency, while the red squares and the green triangles represent the Compton and the total efficiencies, respectively. The results are obtained without 1 mm Al sample holder and 1.5 mm Al crystal housing. The low γ-ray energy determine a much stronger dependence on the detector cross section, rather then its depth. Uncertainties correspond to one standard deviation and reflect statistical uncertainties alone (ranging from 0.01 % to 0.05 %).

Figure 11. Schematic layout of the CIRA GHIBLI Plasma Wind Tunnel. The main sections are shown from left to right: Archeater, nozzles, test chamber with the test article and its support, diffuser, heat exchanger and the vacuum system. The cylindrical 2x2 inch $LaBr_3$(Ce) γ-detector will be placed in the water cooled test article support.

Figure 12. It is shown a purely demonstrative image of a typical PWT test article (left side) where the N temperature and recession rate simultaneous measurements could be made. The trend with time, simulated with numerical tools, represents the final goal of the research program (right side), see text.

$$(2)\int_{\lambda_1}^{\lambda_2} \varepsilon(\lambda,T) * R(\lambda,T) * F_1(\lambda) * P(\lambda,T)\delta\lambda$$

$$(1)\int_0^{\infty} \varepsilon(\lambda,T)P(\lambda,T)\delta\lambda$$

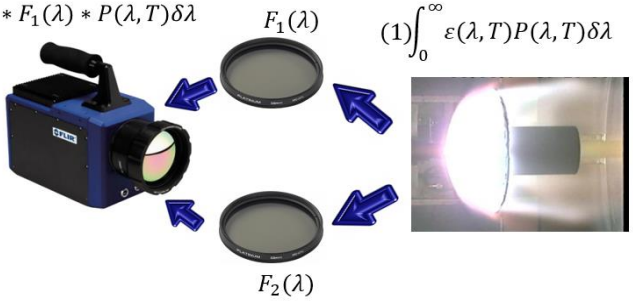

$$(3)\int_{\lambda_1}^{\lambda_2} \varepsilon(\lambda,T) * R(\lambda,T) * F_2(\lambda) * P(\lambda,T)\delta\lambda$$

Figure 1

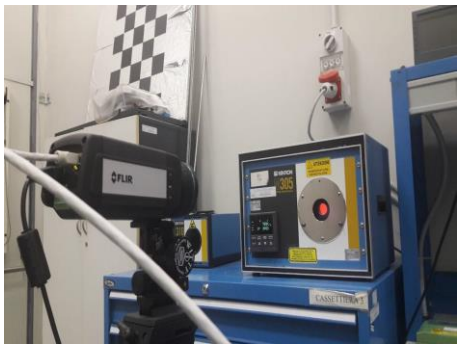

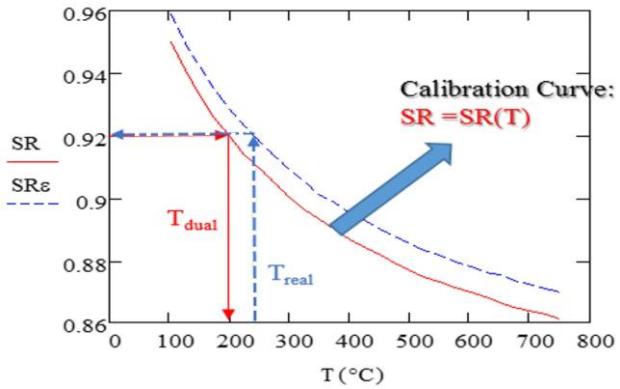

Figure 2

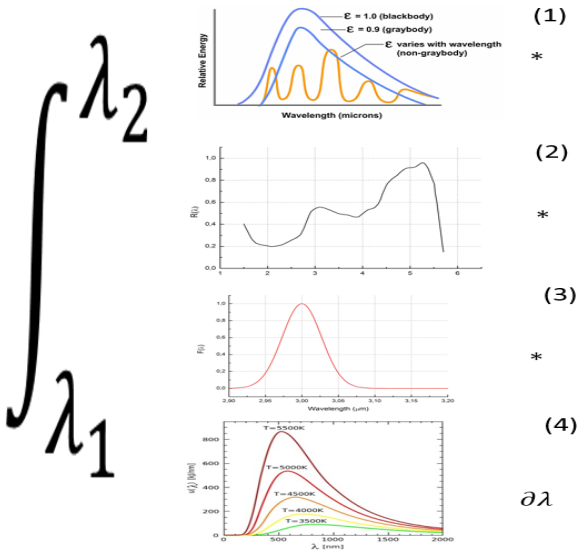

Figure 3

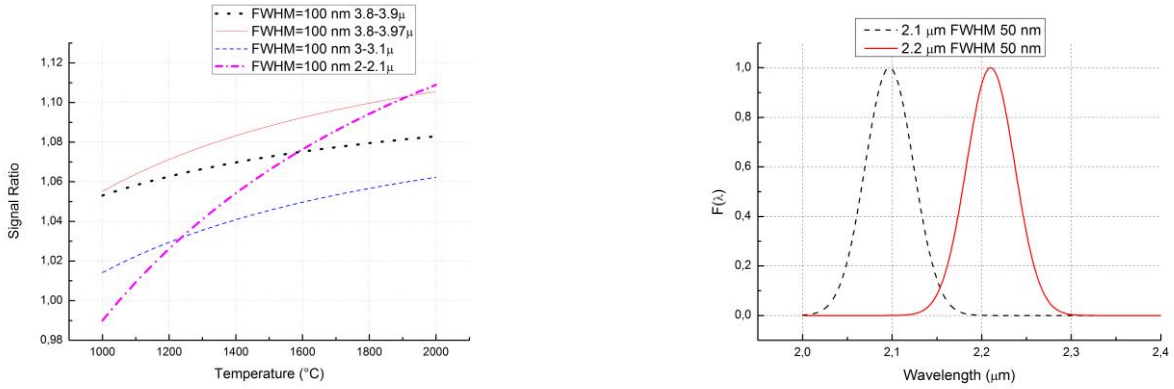

Figure 4

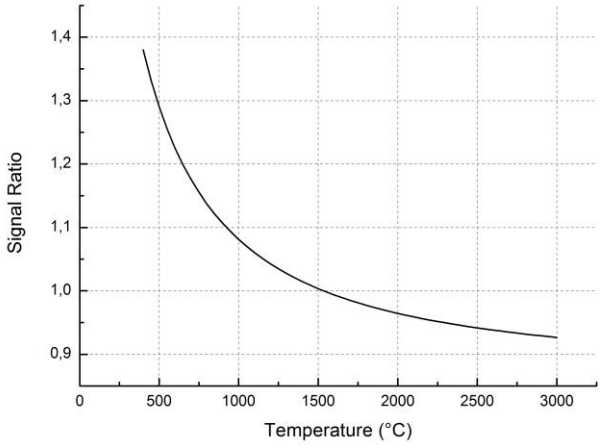

Figure 5

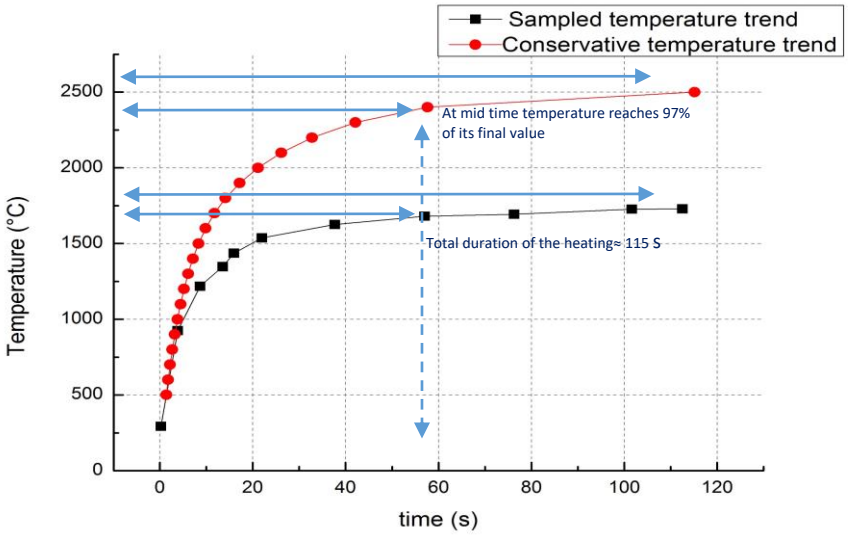

Figure 6

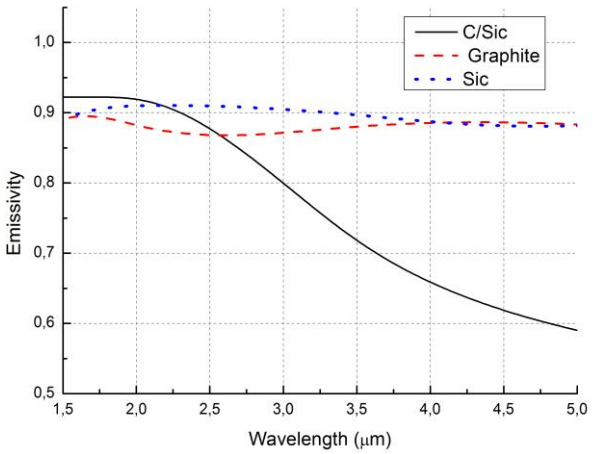

Figure 7

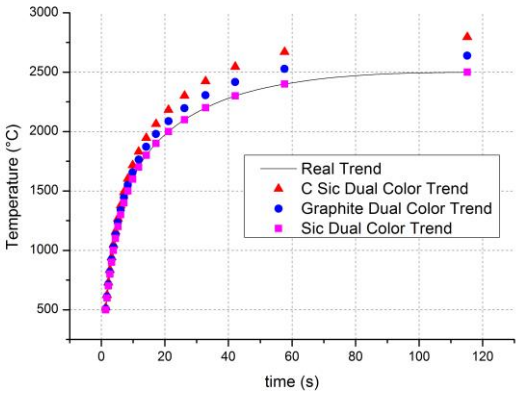

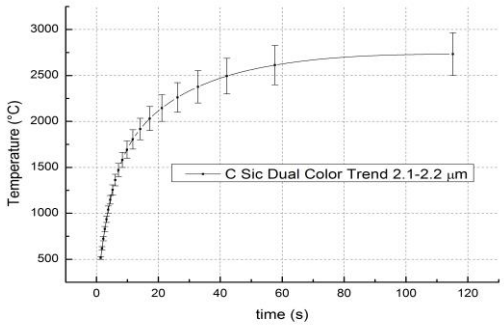

Figure 8

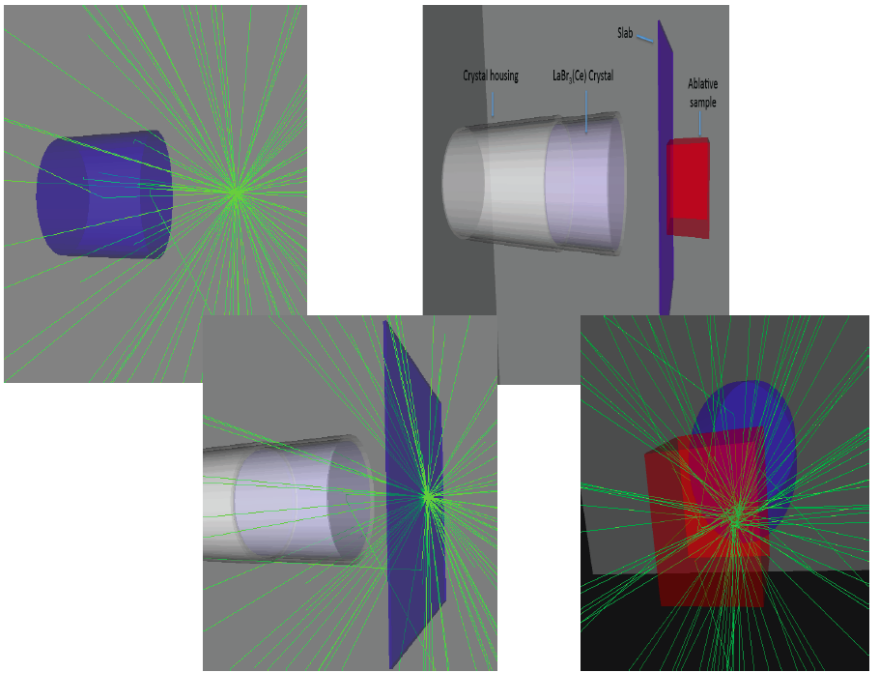

Figure 9

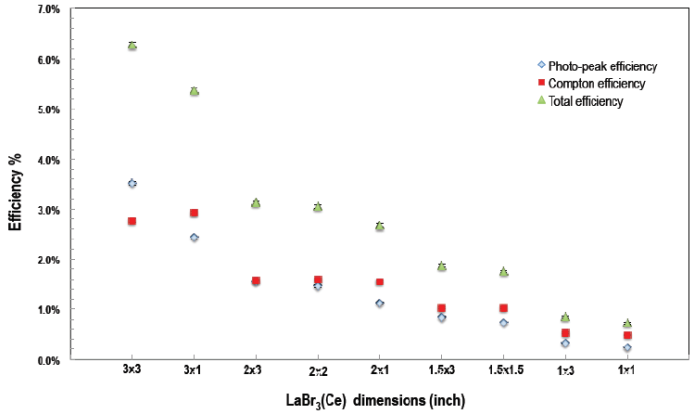

Figure 10

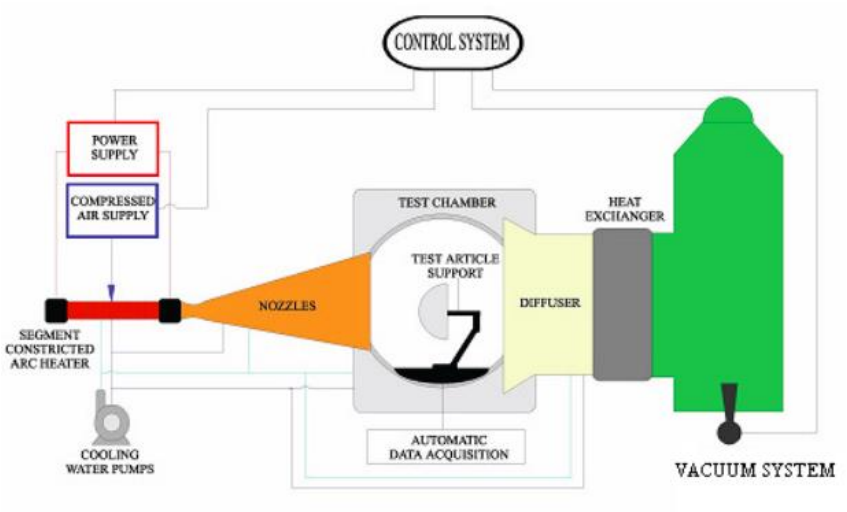

Figure 11

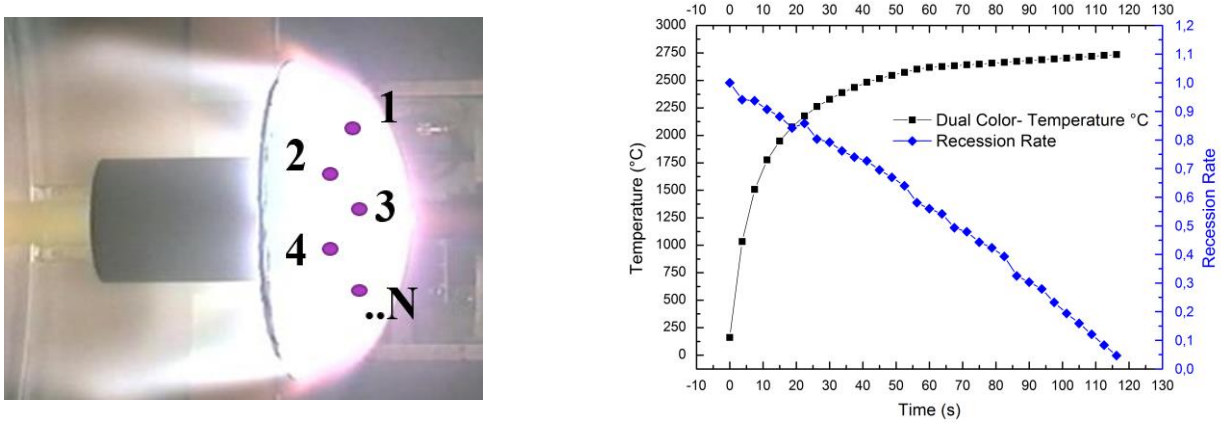

Figure 12